JOURNAL OF COMPUTATIONAL PHYSICS 76, 301–326 (1988)

A Numerical Study of Superfluid Turbulence in the Self-Induction Approximation

THOMAS F. BUTTKE*

Department of Mathematics and Lawrence Berkeley Laboratory, University of California, Berkeley, California 94720

Received March 27, 1987; revised July 2, 1987

Two stable numerical methods are presented to solve the self-induction equation of vortex theory. These numerical methods are validated by comparison with known exact solutions. A new self-similar solution of the self-induction equation is presented and the approximate solutions are shown to converge to the exact solution for the self-similar solution. The numerical method is then generalized to solve the equations of motion of a superfluid vortex in the self-induction approximation where reconnection is allowed. A careful numerical study shows that the mesh spacing of the method must be restricted so that the approximate solutions are accurate. The line length density of a system of superfluid vortices is calculated. Contrary to earlier results it is found that the line length density produced does not scale as the velocity squared and therefore is not characteristic of homogeneous turbulence. It is concluded that the model equation used is inadequate to describe superfluid turbulence.

INTRODUCTION

We present a numerical method which solves the equations of motion for a superfluid vortex in the self-induction approximation. We present the first, as far as we know, stable numerical methods to solve the self-induction equation. The self-induction equation is equivalent to a non-linear Schrödinger equation which has an infinite number of integral invariants. The numerical stability of our methods results from the fact that we preserve three of these invariants. We validate our numerical methods with a careful comparison of known smooth exact solutions with the approximate solutions; we find that one method is second-order accurate in space and time, while the other is fourth-order accurate in space when the time step is appropriately related to the spatial step. We also present a new exact self-similar solution of the Riemann problem for the self-induction equation; we verify that the approximate solutions converge to the exact solution for the self-similar solution. The Riemann problem is particularly interesting because we solve a model equation which incorporates the reconnecton ansatz of Feynman [1] as introduced by Schwarz [2] which introduces the same singularity to the vortex as is present in the Riemann problem.

* Current address: Program in Applied and Computational Mathematics, Princeton University, Princeton, NJ 08544

0021-9991/88 $3.00

A vortex evolving according to the self-induction equation does not stretch or contract and we use this property when solving the self-induction equation; thus we generalize our basic method to solve equations which are perturbations of the self-induction equation which cause the vortex to stretch or contract. We apply our method to an equation proposed by Schwarz [3] which is used with the reconnection ansatz to model the evolution of a superfluid vortex. We find that certain restrictions must be placed on the mesh spacing along the vortex so that the approximate solutions give good approximations to the exact solutions; in the appropriate dimensionless units the condition is that $\Delta\xi$ the mesh spacing must satisfy $\Delta\xi \leqslant 0.5$. We use our method to calculate the equilibrium line length in a cube with periodic boundary conditions. If the line length density is characteristic of homogeneous turbulence the line length density should be proportional to the mean countercurrent velocity squared. Contrary to earlier results we find that the line length density is nearly linearly dependent on the countercurrent velocity; however, we are able to reproduce earlier results when the mesh spacing condition is violated.

The Self-Induction Equation

We consider a line vortex in an infinite three-dimensional incompressible isentropic fluid. The position of the line vortex is given by a function $\mathbf{r}(\xi)$, where ξ is a Lagrangian variable labeling the fluid particles along the vortex. The velocity $\mathbf{u}(\mathbf{x})$ of the fluid at the point $\mathbf{x}$ in the fluid is given by [4]

$$\mathbf{u}(\mathbf{x}) = -\frac{\Gamma}{4\pi}\int_0^{\xi_0} \frac{\mathbf{p}\times \partial\mathbf{r}/\partial\xi}{|\mathbf{p}|^3}\, d\xi, \tag{1}$$

where $\mathbf{p} \equiv \mathbf{x} - \mathbf{r}(\xi)$, Γ is the strength of the vortex, and the integration is carried out along the entire vortex. Since the vortex moves with the local fluid velocity, Eq. (1) formally determines the evolution of the vortex when we evaluate the fluid velocity on the line vortex itself. However, as $\mathbf{x}$ approaches the line vortex $|\mathbf{p}| \to 0$ and the integral in Eq. (1) diverges. In order to determine the behavior of the velocity as $\mathbf{x}$ approaches the vortex a formal expansion of the integrand can be carried out [5, 6, 7]. The result is

$$\mathbf{u}(\mathbf{x}_0) \approx \frac{\Gamma}{4\pi}\log\frac{L}{\sigma}\,\mathbf{r}'\times\mathbf{r}'' + O(1), \tag{2}$$

where σ is the distance from the point of observation $\mathbf{x}_0$ to the line vortex, $'$ denotes the derivative with respect to arclength measured along the vortex, L is a small fixed length, and $O(1)$ indicates the terms of lower order in σ which have been ignored. σ is generally chosen equal to some multiple of the radius of the vortex and the lower order terms are ignored. Equation (2) is called the self-induction approximation. The approximation is not a good approximation for long times

since the ignored terms are generally comparable to the term which remains. Furthermore, as we shall see shortly, the self-induction approximation allows for no stretching of the vortex; this is in contrast to the stretching which occurs when the nonlocal terms are not ignored [8, 9]. The main attribute of the self-induction approximation is the fact that it is a local approximation; this is the reason that the approximation is so widely used in vortex dynamics.

From Eq. (2) we obtain the equation of motion for a vortex in the self-induction approximation:

$$\frac{\partial \mathbf{r}}{\partial t} = \beta \mathbf{r}' \times \mathbf{r}'', \tag{3}$$

where t is time, $\beta = (\Gamma/4\pi)\log(L/\sigma)$. Without loss of generality we choose $\beta = 1.0$. We first show that a vortex evolving according to Eq. (3) does not stretch or contract. Define $\mathbf{g} \equiv \partial \mathbf{r}/\partial \xi$ and $g \equiv |\mathbf{g}|$, then we have that $g = \partial s/\partial \xi$ and $\partial/\partial \xi = g\,\partial/\partial s$, where s denotes arclength measured along the vortex. If we differentiate the terms of Eq. (3) with respect to ξ we find

$$\frac{\partial \mathbf{g}}{\partial t} = \mathbf{g} \times \frac{\partial^3 \mathbf{r}}{\partial s^3}. \tag{4}$$

If take the inner product of Eq. (4) with $\mathbf{g}$ we have

$$\frac{\partial g}{\partial t} = 0. \tag{5}$$

Since

$$s = \int_0^{\xi} g\, d\tilde{\xi},$$

Eq. (5) tells us that $\partial s/\partial t = 0$, i.e., the vortex does not stretch or contract. s depends only on the initial Lagrangian parametrization of the vortex and is independent of time; thus we may choose the arclength as a Lagrangian parametrization of the vortex. If we parametrize the vortex in terms of the arclength Eq. (4) becomes

$$\frac{\partial \boldsymbol{l}}{\partial t} = \boldsymbol{l} \times \frac{\partial^2 \boldsymbol{l}}{\partial s^2}, \tag{6}$$

where $\boldsymbol{l} \equiv \partial \mathbf{r}/\partial s$ is the unit tangent to the vortex and $\mathbf{g} = g\boldsymbol{l}$. Equation (6) is equivalent to Eq. (3) in the following sense: if $\boldsymbol{l}(s, t)$ is a solution of Eq. (6) then $\mathbf{r}(s, t)$ is a solution of Eq. (3) if we define $\mathbf{r}$ as

$$\mathbf{r}(s, t) = \mathbf{r}(0, 0) + \int_0^t (\boldsymbol{l}(0, \eta) \times \boldsymbol{l}'(0, \eta))\, d\eta + \int_0^s (\boldsymbol{l}(\zeta, t) \times \boldsymbol{l}''(\zeta, t))\, d\zeta, \tag{7}$$

where $' = \partial/\partial s$. The fact that $\mathbf{r}(s, t)$, as given by Eq. (7), is a solution of Eq. (3) can be verified by substitution of the appropriate derivatives into Eq. (3).

We use Eq. (6) to solve for $\boldsymbol{l}$ rather than use Eq. (3) to solve for $\mathbf{r}$ directly for the following reasons. Solutions of Eq. (6) satisfy the constraint that $|\boldsymbol{l}| = 1$. Thus we see that the motion of the vortex is really determined by only two independent quantities. We are able to design our numerical methods so that $|\boldsymbol{l}| = 1$ numerically as well; whereas if we were to use Eq. (3) it is not obvious how to impose a similar constraint. This observation seems to be key in developing stable schemes to solve the self-induction equation. If the constraint is not imposed on the numerical methods then one component of the motion of the vortex is undetermined and the undetermined component will grow in an unstable manner.

Hasimoto [10] shows that Eq. (6) is equivalent to the non-linear Schrödinger equation:

$$\frac{1}{i}\frac{\partial \psi}{\partial t} = \frac{\partial^2 \psi}{\partial s^2} + \frac{1}{2}\psi |\psi|^2, \tag{8}$$

where ψ is a complex scalar function related to the curvature and torsion of the vortex. Equation (8) is a soliton equation which has an infinite number of integral invariants. The simplest of these invariants, which we take from Newell [11], is

$$\frac{d}{dt}\int |\psi|^2 \, ds = \frac{d}{dt}\int |\boldsymbol{l}'|^2 \, ds = 0. \tag{9}$$

In addition to the scalar invariants of the Schrödinger equation, Eq. (3) has at least one vector invariant for closed vortices. Define $\mathbf{A} \equiv \frac{1}{2}\int \mathbf{r} \times \boldsymbol{l} \, ds$, where the integration is carried out along a closed vortex. If the vortex lies in a plane, $|\mathbf{A}|$ is equal to the area enclosed by the vortex and $\mathbf{A}$ points in a direction normal to the plane in which the vortex lies. We show that for a closed vortex evolving according to Eq. (3) $d\mathbf{A}/dt = 0$. From the definition of $\mathbf{A}$ we have

$$\begin{aligned}\frac{d\mathbf{A}}{dt} &= \frac{1}{2}\int \left(\frac{\partial \mathbf{r}}{\partial t} \times \boldsymbol{l} + \mathbf{r} \times \frac{\partial \boldsymbol{l}}{\partial t}\right) ds \\ &= \frac{1}{2}\int ((\boldsymbol{l} \times \boldsymbol{l}') \times \boldsymbol{l} + \mathbf{r} \times (\boldsymbol{l} \times \boldsymbol{l}'')) \, ds \\ &= \int (\boldsymbol{l} \times \boldsymbol{l}') \times \boldsymbol{l} \, ds = \int \boldsymbol{l}' \, ds = 0,\end{aligned} \tag{10}$$

where in the second equality we have used Eqs. (3) and (6), and in the third equality we have integrated by parts. An immediate consequence of (10) is the fact that circular vortices remain circularly shaped as they evolve according to the self-induction equation.

Exact Solutions of the Self-Induction Equation

Vortices in the shapes of circles, helices, or lines evolve according to Eq. (3) so that their initial shape remains unchanged as they propagate. A family of exact solutions of Eq. (6), known as solitons, can be generated by considering solutions of the non-linear Schrödinger equation. Hasimoto [10] writes down an explicit formula for a soliton on a vortex; the vortex has constant torsion τ and its curvature κ is given by $\kappa^2 = 4\nu^2 \operatorname{sech}^2 \nu(s - 2\tau t)$, where ν is a constant. The corresponding equation for the tangent $\boldsymbol{l}$ of the vortex, written in its cartesian components, is

$$\begin{aligned} l_x &= 1 - 2\mu \operatorname{sech}^2 \eta, \\ l_1 + i l_2 &= -2\mu \operatorname{sech} \eta (\tanh \eta - iT) e^{i\Theta}, \end{aligned} \tag{11}$$

where $\eta = \nu(s - 2\tau t)$, $T = \tau/\nu$, $\Theta = T\eta + (\nu^2 + \tau^2)\, t$, and $\mu = 1/(1 + T^2)$. The vortex is oriented so that the tangent is parallel to the x-axis at $s = \pm\infty$. We use this family of solutions for verifying our numerical schemes for smooth solutions.

We now present a new exact solution of Eq. (6). The solution is self-similar and solves the Riemann problem:

$$\boldsymbol{l}(s, 0) = \begin{cases} \boldsymbol{l}_+ & \text{if } s > 0 \\ \boldsymbol{l}_- & \text{if } s < 0, \end{cases} \tag{12}$$

where $\boldsymbol{l}_+$ and $\boldsymbol{l}_-$ are constant unit vectors. Consider a solution $\boldsymbol{l}(s, t)$ of Eq. (6) with initial conditions (12) under the coordinate transformation $\tilde{s} = s/\alpha$ and $\tilde{t} = t/\beta$. We find that

$$\frac{\alpha^2}{\beta} \frac{\partial \boldsymbol{l}}{\partial \tilde{t}} = \boldsymbol{l} \times \frac{\partial^2 \boldsymbol{l}}{\partial \tilde{s}^2}. \tag{13}$$

If we let $\alpha = \sqrt{\beta}$ then Eq. (6) is identical to Eq. (13) and since the initial conditions (12) are invariant under the coordinate transformation we are considering, we find $\boldsymbol{l}(s, t) = \boldsymbol{l}(s/\sqrt{\beta}, t/\beta)$ for all β. By choosing $\beta = t$ we find that $\boldsymbol{l}$ is a function of the self-similar variable $\eta = s/\sqrt{t}$. When we substitute $\boldsymbol{l}(\eta)$ into Eq. (6) we find that $\boldsymbol{l}$ satisfies

$$\eta \frac{d\boldsymbol{l}}{d\eta} = 2 \frac{d^2 \boldsymbol{l}}{d\eta^2} \times \boldsymbol{l}, \tag{14}$$

where $\eta = s/\sqrt{t}$.

We can solve Eq. (14) by use of the Frenet–Serret formulae. The Frenet–Serret formulae depend only on the fact that we have a smooth parametrization of a unit vector. Let $\boldsymbol{l}(\xi)$ be a unit vector and define $\kappa_\xi \equiv \pm |d\boldsymbol{l}/d\xi|$. We define $\mathbf{n}_\xi$ to be a continuous unit vector such that $\kappa_\xi \mathbf{n}_\xi = d\boldsymbol{l}/d\xi$ and since $\boldsymbol{l} \cdot d\boldsymbol{l}/d\xi = 0$ we define $\mathbf{b}_\xi \equiv \boldsymbol{l} \times \mathbf{n}_\xi$ to give us the third member of the orthonormal triad. Define $\tau_\xi \equiv \mathbf{b}_\xi \cdot d\mathbf{n}_\xi/d\xi$. We use the subscrit ξ to emphasize the fact that the defined quantities depend on the

particular parametrization of $\boldsymbol{l}$ that we use. We immediately write down the Frenet–Serret formulae:

$$\frac{d}{d\xi}\begin{bmatrix}\boldsymbol{l}\\ \mathbf{n}_\xi\\ \mathbf{b}_\xi\end{bmatrix}=\begin{bmatrix}0 & \kappa_\xi & 0\\ -\kappa_\xi & 0 & \tau_\xi\\ 0 & -\tau_\xi & 0\end{bmatrix}\begin{bmatrix}\boldsymbol{l}\\ \mathbf{n}_\xi\\ \mathbf{b}_\xi\end{bmatrix}, \tag{15}$$

where we have used the definitions given above; and we have used the orthogonality relations between the vectors to obtain the fact that the matrix in Eq. (15) must be of the form given.

We rewrite Eq. (14) by repeated use of Eq. (15) to obtain

$$\eta\kappa_\eta\mathbf{n}_\eta=-2\frac{d\kappa_\eta}{d\eta}\mathbf{b}_\eta+2\kappa_\eta\tau_\eta\mathbf{n}_\eta. \tag{16}$$

From Eq. (16) we see that $\kappa_\eta=\kappa_0$ a constant, and since we assume $\kappa_0\neq 0$. (If $\kappa_0=0$ the solution reduces to the trivial straight vortex case.) We have $\tau_\eta=\eta/2$. We now relate the true curvature and torsion κ_s and τ_s to κ_η and τ_η. Since $\partial/\partial s=(1/\sqrt{t})(d/d\eta)$ we have

$$\kappa_s\cdot\mathbf{n}_s=\frac{\partial\boldsymbol{l}}{\partial s}=\frac{1}{\sqrt{t}}\frac{d\boldsymbol{l}}{d\eta}=\frac{\kappa_\eta}{\sqrt{t}}\mathbf{n}_\eta. \tag{17}$$

From Eq. (17) we deduce two facts: (1) $\mathbf{n}_s=\mathbf{n}_\eta$ and thus $\mathbf{b}_s=\mathbf{b}_\eta$; (2) $\kappa=\kappa_0/\sqrt{t}$, where we denote the true curvature κ_s by κ. From the definitions of τ_s and τ_η and from the fact that $\mathbf{b}_s=\mathbf{b}_\eta$ we obtain that $\tau=\tau_\eta/\sqrt{t}=s/2t$, where we denote the true torsion τ_s by τ. We have obtained that the solution to Eq. (6) with initial conditions (12) is the vortex specified by

$$\kappa=\frac{\kappa_0}{\sqrt{t}}\qquad\text{and}\qquad\tau=\frac{s}{2t}, \tag{18}$$

where κ and τ are the curvature and torsion of the vortex, and κ_0 is a constant determined by the angle between $\boldsymbol{l}_+$ and $\boldsymbol{l}_-$ [12]. We note that initially the curvature of the vortex is zero everywhere along the vortex except for a Dirac mass at the origin; at positive times the curvature is constant along the vortex; this behaviour is indicative of the fact that waves can travel with an infinite speed along a vortex whose evolution is governed by the self-induction equation. We use this solution when verifying our secnd-order numerical scheme for singular initial data.

The Finite Difference Equations for Self-Induction

In this section we introduce a finite difference approximation of Eq. (6) which is second-order accurate in space and time. We present three invariants of the

equations and we present a method for solving the non-linear difference equations which shows that solutions of the finite difference equations can be found for all times and for all initial conditions. We also present a method which is second-order accurate in time and fourth-order accurate in space which produces approximate solutions which satisfy the same invariants as do solutions of the second-order scheme.

Let $\boldsymbol{l}_j^n$ denote the approximation to $\boldsymbol{l}(j\,\Delta s, n\,\Delta t)$ which satisfies

$$\boldsymbol{l}_j^{n+1} - \boldsymbol{l}_j^n = \frac{\Delta t}{4(\Delta s)^2}(\boldsymbol{l}_j^n + \boldsymbol{l}_j^{n+1}) \times (\boldsymbol{l}_{j-1}^n + \boldsymbol{l}_{j-1}^{n+1} + \boldsymbol{l}_{j+1}^n + \boldsymbol{l}_{j+1}^{n+1}), \tag{19}$$

where Δs is the spatial increment and Δt is the temporal increment. Equation (19) is a Crank–Nicholson type scheme. The second term on the right side of (19) is the second-order centered difference approximation for second-order derivatives, in which the missing term has been cancelled by the first term in the cross product. Solutions of Eq. (19) have three invariants,

$$|\boldsymbol{l}_j^{n+1}| = |\boldsymbol{l}_j^n|, \tag{20}$$

$$\sum_{j=1}^{j=N} \boldsymbol{l}_j^{n+1} = \sum_{j=1}^{j=N} \boldsymbol{l}_j^n, \tag{21}$$

$$\sum_{j=1}^{j=N} |\boldsymbol{l}_j^{n+1} - \boldsymbol{l}_{j-1}^{n+1}|^2 = \sum_{j=1}^{j=N} |\boldsymbol{l}_j^n - \boldsymbol{l}_{j-1}^n|^2, \tag{22}$$

where $\boldsymbol{l}_j^n$ satisfies periodic boundary conditions. The first invariant (20) guarantees that there is no local stretching of the vortex which is also true for solutions of Eq. (6): $\boldsymbol{l}$ is a unit vector for all times and Eq. (20) shows that $|\boldsymbol{l}_j^n|$ is a unit vector for all n provided that it has unit magnitude initially. The second invariant (21) guarantees that a closed vortex remains a closed vortex. The third invariant (22) corresponds to the invariant of Eq. (6)

$$\frac{d}{dt}\int |\boldsymbol{l}'|^2\, ds = 0.$$

where $' = \partial/\partial s$.

We present two iterative methods for solving the finite difference equation (19). Both methods produce a sequence of unit vectors $\mathbf{x}_j^k$ which converge to $\boldsymbol{l}_j^{n+1}$, the unique solution of (19), provided Δt is appropriately restricted. Both methods converge independently of the initial conditions. In the first method we define the sequence iteratively as follows. Assume we are given any $\boldsymbol{l}_j^n$ of unit magnitude, then define $\mathbf{y}_j^{k+1}$ by the equation

$$\mathbf{y}_j^{k+1} - \boldsymbol{l}_j^n = \frac{\Delta t}{4(\Delta s)^2}(\boldsymbol{l}_j^n + \mathbf{x}_j^k) \times (\boldsymbol{l}_{j-1}^n + \mathbf{x}_{j-1}^k + \boldsymbol{l}_{j+1}^n + \mathbf{x}_{j+1}^k), \tag{23}$$

and then define

$$\mathbf{x}_j^{k+1} \equiv \frac{\mathbf{y}_j^{k+1}}{|\mathbf{y}_j^{k+1}|}. \tag{24}$$

If we require $\Delta t/\Delta s^2 < \frac{1}{4}$ it can be shown that the sequence $\mathbf{x}_j^k$ defined by Eqs. (23) and (24) converges to $\boldsymbol{l}_j^{n+1}$; furthermore, the analysis shows the solution of (19) is unique [12]. The restriction on $\Delta t/\Delta s^2$ guarantees that the sequence $\mathbf{x}_j^k$ is always well defined and converges for any $\mathbf{x}_j^0$ of unit magnitude; however, we always choose $\mathbf{x}_j^0 = \boldsymbol{l}_j^n$.

In order to define the sequence $\mathbf{x}_j^k$ for the second method we first solve the linear equation

$$\mathbf{x} + \mathbf{b} \times \mathbf{x} = \boldsymbol{l} + \boldsymbol{l} \times \mathbf{b}, \tag{25}$$

for $\mathbf{x}$ in terms of the other vectors. The solution to Eq. (25) is

$$\mathbf{x}(1 + |\mathbf{b}|^2) = \boldsymbol{l}(1 - |\mathbf{b}|^2) + 2(\boldsymbol{l} \times \mathbf{b}) + 2\mathbf{b}(\boldsymbol{l} \cdot \mathbf{b}). \tag{26}$$

We note that $|\mathbf{x}| = |\boldsymbol{l}|$; this fact guarantees that the vectors of the sequence, which we define shortly, are of unit magnitude. We define the sequence of unit vectors $\mathbf{x}_j^k$ iteratively by the equation

$$\mathbf{x}_j^{k+1} - \boldsymbol{l}_j^n = \frac{\Delta t}{4(\Delta s)^2}(\boldsymbol{l}_j^n + \mathbf{x}_j^{k+1}) \times (\boldsymbol{l}_{j-1}^n + \mathbf{x}_{j-1}^k + \boldsymbol{l}_{j+1}^n + \mathbf{x}_{j+1}^k). \tag{27}$$

Equation (27) can be written in the form of Eq. (25) in order to solve for $\mathbf{x}_j^{k+1}$. We assume that $|\boldsymbol{l}_j^n| = 1$ and thus we have a sequence of unit vectors $\mathbf{x}_j^k$. If we restrict $\Delta t/\Delta s^2 < 1$ it can be shown that the sequence $\mathbf{x}_j^k$ converges to $\boldsymbol{l}_j^{n+1}$ the unique solution of Eq. (19); furthermore, the solution exists for all $\boldsymbol{l}_j^n$ [12].

Invariants (20) and (22) show that the numerical method is stable in the $\mathbf{H}_0^1$ norm $\|\cdot\|_1$ defined as

$$\|l^n\|_1^2 = \Delta s \sum_{j=1}^{j=N} |\boldsymbol{l}_j^n|^2 + \Delta s \sum_{j=1}^{j=N} \frac{|\boldsymbol{l}_j^n - \boldsymbol{l}_{j-1}^n|^2}{\Delta s^2},$$

where we denote by l^n the $3N$ component solution vector of Eq. (19) at the time step n made up of the $\boldsymbol{l}_j^n$. The numerical method is stable since from (20) and (22) we have $\|l^n\|_1 = \|l^0\|_1$.

The method defined by Eq. (19) is formally second-order accurate in space and second-order accurate in time. If we solve the finite difference equations by Eq. (27) we must place the restriction $\Delta t < \Delta s^2$ on the time step; thus the overall method is limited by the second-order accuracy in the space discretization. We obtain a method which is formally fourth-order accurate overall in Δs by replacing the second-order spatial approximation in Eq. (19) by the fourth-order centered

difference approximation. The fourth-order approximation is defined by requiring that it satisfy

$$\boldsymbol{l}_j^{n+1} - \boldsymbol{l}_j^n = \frac{\Delta t}{\Delta s^2} \boldsymbol{l}_j^{\text{ave}} \times \left(\frac{4}{3} (\boldsymbol{l}_{j-1}^{\text{ave}} + \boldsymbol{l}_{j+1}^{\text{ave}}) - \frac{1}{12} (\boldsymbol{l}_{j-2}^{\text{ave}} + \boldsymbol{l}_{j+2}^{\text{ave}}) \right), \tag{28}$$

where $\boldsymbol{l}_j^{\text{ave}} \equiv (\boldsymbol{l}_j^n + \boldsymbol{l}_j^{n+1})/2$. The finite difference equations (28) can be solved by the method analogous to the one given in Eq. (27); the condition $\Delta t/\Delta s^2 < \frac{12}{17}$ guarantees that the solutions exist and are unique [12]. Solutions of Eq. (28) also have three invariants,

$$\begin{gathered} |\boldsymbol{l}_j^{n+1}| = |\boldsymbol{l}_j^n|, \\ \sum_{j=1}^{j=N} \boldsymbol{l}_j^{n+1} = \sum_{j=1}^{j=N} \boldsymbol{l}_j^n, \end{gathered} \tag{29}$$

$$\frac{4}{3} \sum_{j=1}^{j=N} |\boldsymbol{l}_j^{n+1} - \boldsymbol{l}_{j-1}^{n+1}|^2 - \frac{1}{12} \sum_{j=1}^{j=N} |\boldsymbol{l}_{j+1}^{n+1} - \boldsymbol{l}_{j-1}^{n+1}|^2 = \frac{4}{3} \sum_{j=1}^{j=N} |\boldsymbol{l}_j^n - \boldsymbol{l}_{j-1}^n|^2 - \frac{1}{12} \sum_{j=1}^{j=N} |\boldsymbol{l}_{j+1}^n - \boldsymbol{l}_{j-1}^n|^2, \tag{30}$$

where $\boldsymbol{l}_j^n$ satisfies periodic boundary conditions. Equation (30) is the fourth-order analog of Eq. (22). Method (28) is stable in the H_0^1 norm $\|\cdot\|_1$ defined as

$$\|l^n\|_1^2 = \Delta s \sum_{j=1}^{j=N} |\boldsymbol{l}_j^n|^2 + \frac{4}{3} \Delta s \sum_{j=1}^{j=N} \frac{|\boldsymbol{l}_j^n - \boldsymbol{l}_{j-1}^n|^2}{\Delta s^2} - \frac{1}{3} \Delta s \sum_{j=1}^{j=N} \frac{|\boldsymbol{l}_{j+1}^n - \boldsymbol{l}_{j-1}^n|^2}{4(\Delta s)^2},$$

where l^n is the $3N$ component solution vector of (28) made up of the $\boldsymbol{l}_j^n$. Method (28) is stable since from Eq. (29) and Eq. (30) we have that $\|l^n\|_1 = \|l^0\|_1$.

Given an approximation to the tangent field of the vortex we now determine an approximation to the position of the vortex $\mathbf{r}(s, t)$. Our approximation of $\mathbf{r}(s, t)$ is based on Eq. (7). We use second-order integration methods in evaluating the integrals in Eq. (7) to maintain second-order accuracy. Let $\mathbf{u}$ denote the velocity of the vortex; then we have

$$\mathbf{u}(s, t) \equiv \frac{\partial \mathbf{r}}{\partial t} = \boldsymbol{l} \times \frac{\partial \boldsymbol{l}}{\partial s}.$$

Let $\mathbf{u}_j^{n+1/2}$ denote the approximation of $\mathbf{u}(j\,\Delta s, (n+\frac{1}{2})\,\Delta t)$ defined by

$$\mathbf{u}_j^{n+1/2} \equiv \frac{1}{2\Delta s} \boldsymbol{l}_j^{\text{ave}} \times (\boldsymbol{l}_{j+1}^{\text{ave}} - \boldsymbol{l}_{j-1}^{\text{ave}}), \tag{31}$$

where $\boldsymbol{l}_j^{\text{ave}} \equiv (\boldsymbol{l}_j^{n+1} + \boldsymbol{l}_j^n)/2$. Using equations (7) and (29) we obtain $\mathbf{r}_j^n$, the approximation to $\mathbf{r}(j\,\Delta s, n\,\Delta t)$:

$$\mathbf{r}_j^n \equiv \mathbf{r}_0^0 + \Delta t \sum_{m=1}^{n} (\mathbf{u}_0^{m-1/2}) + \frac{\Delta s}{2} \sum_{i=1}^{j} (\boldsymbol{l}_i^n + \boldsymbol{l}_{i-1}^n). \tag{32}$$

Approximation (32) gives us a self-consistency property for the motion of a point on the vortex. This consistency property is the fact that the calculated position in 3-space of a particle on the vortex is independent of where on the vortex we calculate the velocity numerically, provided we use Eq. (19) and (31) as the defining equations for $\boldsymbol{l}_j^n$ and $\mathbf{u}_j^n$. In order to verify this consistency property we show that the motion of a particle is given by

$$\mathbf{r}_j^{n+1} - \mathbf{r}_j^n = \Delta t\, \mathbf{u}_j^{n+1/2}, \tag{33}$$

for all j and n where $\mathbf{u}_j^{n+1/2}$ is defined by Eqs. (31) and (19), and $\mathbf{r}_j^n$ is given by Eq. (32). Using the definition of $\mathbf{r}_j^n$ we obtain

$$\begin{aligned}
\mathbf{r}_j^{n+1} - \mathbf{r}_j^n &= \Delta t\, \mathbf{u}_0^{n+1,2} + \frac{\Delta s}{2} \sum_{i=1}^{j} (\boldsymbol{l}_i^{n+1} - \boldsymbol{l}_i^n + \boldsymbol{l}_{i-1}^{n+1} - \boldsymbol{l}_{i-1}^n) \\
&= \Delta t\, \mathbf{u}_0^{n+1,2} + \frac{\Delta t}{2\Delta s} \sum_{i=1}^{j} (\boldsymbol{l}_i^{\text{ave}} \times (\boldsymbol{l}_{i+1}^{\text{ave}} + \boldsymbol{l}_{i-1}^{\text{ave}}) + \boldsymbol{l}_{i-1}^{\text{ave}} \times (\boldsymbol{l}_i^{\text{ave}} + \boldsymbol{l}_{i-2}^{\text{ave}})) \\
&= \Delta t\, \mathbf{u}_0^{n+1,2} + \frac{\Delta t}{2\Delta s} \sum_{i=1}^{j} (\boldsymbol{l}_i^{\text{ave}} \times (\boldsymbol{l}_{i+1}^{\text{ave}} - \boldsymbol{l}_{i-1}^{\text{ave}}) - \boldsymbol{l}_{i-1}^{\text{ave}} \times (\boldsymbol{l}_i^{\text{ave}} - \boldsymbol{l}_{i-2}^{\text{ave}})) \\
&= \Delta t\, \mathbf{u}_0^{n+1,2} + \Delta t \sum_{i=1}^{j} (\mathbf{u}_i^{n+1\,2} - \mathbf{u}_{i-1}^{n+1/2}) \\
&= \Delta t\, \mathbf{u}_j^{n+1/2},
\end{aligned} \tag{34}$$

where in the second equality we use Eq. (19), in the fourth equality we use Eq. (31) and we use the notation $\boldsymbol{l}_i^{\text{ave}} = (\boldsymbol{l}_i^{n+1} + \boldsymbol{l}_i^n)/2$.

We summarize our basic second-order method for obtaining approximate solutions to Eq. (3). We solve Eq. (19) by means of Eq. (27) in order to obtain $\boldsymbol{l}_j^n$ the approximate solutions of Eq. (6); we then use Eqs. (31) and (32) to find $\mathbf{r}_j^n$, the second-order approximate solutions of Eq. (3).

An analoguous method is used to obtain the fourth-order approximations, except for the fact that our approximations are chosen to be fourth-order accurate in space. We write the analog to Eq. (32) using a symmetric fourth-order integration formula. We define $\mathbf{r}_j^n$, the fourth-order approximation to $\mathbf{r}(j\,\Delta s, n\,\Delta t)$, as

$$\mathbf{r}_j^n \equiv \mathbf{r}_0^0 + \Delta t \sum_{m=1}^{n} (\mathbf{u}_0^{m-1/2}) + \frac{\Delta s}{24} \sum_{i=1}^{j} (-\boldsymbol{l}_{i+1}^n + 13\boldsymbol{l}_i^n + 13\boldsymbol{l}_{i-1}^n - \boldsymbol{l}_{i-2}^n), \tag{35}$$

where the $\boldsymbol{l}_j^n$ are solutions of Eq. (28). We define $\mathbf{u}_j^{n+1/2}$ so that it is a fourth-order (in space) approximation to $\mathbf{u}(s, t)$ and so that it satisfies Eq. (33). We find that $\mathbf{u}_j^{n+1/2}$, the approximation to $\mathbf{u}(j\,\Delta s, (n+\frac{1}{2})\,\Delta t)$, is defined by

$$\mathbf{u}_j^{n+1/2} \equiv \frac{1}{\Delta s}\left(\frac{13}{18}\boldsymbol{l}_j^{\text{ave}} \times (\boldsymbol{l}_{j+1}^{\text{ave}} - \boldsymbol{l}_{j-1}^{\text{ave}}) - \frac{1}{24}\boldsymbol{l}_j^{\text{ave}} \times (\boldsymbol{l}_{j+2}^{\text{ave}} - \boldsymbol{l}_{j-2}^{\text{ave}})\right.$$
$$\frac{13}{144}(\boldsymbol{l}_{j-1}^{\text{ave}} \times \boldsymbol{l}_{j+1}^{\text{ave}}) - \frac{1}{18}(\boldsymbol{l}_{j-2}^{\text{ave}} \times \boldsymbol{l}_{j-1}^{\text{ave}} + \boldsymbol{l}_{j+1}^{\text{ave}} \times \boldsymbol{l}_{j+2}^{\text{ave}})$$
$$\left. + \frac{1}{288}(\boldsymbol{l}_{j-3}^{\text{ave}} \times \boldsymbol{l}_{j-1}^{\text{ave}} + \boldsymbol{l}_{j+1}^{\text{ave}} \times \boldsymbol{l}_{j+3}^{\text{ave}})\right), \tag{36}$$

where $\boldsymbol{l}_j^{\text{ave}} \equiv (\boldsymbol{l}_j^{n+1} + \boldsymbol{l}_j^n)/2$. We note that each term in Eq. (36) is a second-order approximation to $\boldsymbol{l} \times \boldsymbol{l}'$ while the sum is a fourth-order approximation to $\boldsymbol{l} \times \boldsymbol{l}'$. We can show, using the analogous procedure as shown in Eq. (34), that

$$\mathbf{r}_j^{n+1} - \mathbf{r}_j^n = \Delta t\, \mathbf{u}_j^{n+1/2},$$

for all j and n, where $\mathbf{r}_j^n$ and $\mathbf{u}_j^{n+1/2}$ are defined by Eq. (36), Eq. (35), and Eq. (28); thus the fourth-order method has the same invariants and consistency property as the second-order method.

We summarize our basic fourth-order method for finding approximate solutions to Eq. (3). We solve Eq. (28) by means of the method outlined by Eqs. (25)–(27) to find $\boldsymbol{l}_j^n$; we then use Eqs. (35) and (36) to find $\mathbf{r}_j^n$, the fourth-order approximate solutions to Eq. (3).

Numerical Results for Self-Induction

In this section we compare the approximate solutions obtained by Eq. (19) with the exact solutions given by Eq. (11) for several values of ν and τ, the parameters of Eq. (11). We find that Eq. (19) produces approximate solutions which are second-order accurate in both space and time for smooth solutions. We also verify that the approximate solutions obtained with Eq. (19) converge to the exact solution for the discontinuous initial conditions of the self-similar solution given by Eq. (12). We also verify that the approximate solutions obtained from Eq. (28) are fourth-order accurate in space when we take $\Delta t = c\,\Delta s^2$, where $c < \frac{12}{17}$ is a constant, by comparing them to exact solutions of Eq. (11).

In order to verify the accuracy of the approximate solutions we use the exact solutions given by Eq. (11) for several different values of the parameters ν and τ. We pick the initial conditions so that the exact and approximate solutions are equal at the approximation points initially. We find that the error for the second-order method satisfies $E \approx C_1\,\Delta s^2 + C_2\,\Delta t^2$, where C_1 and C_2 depend on ν and τ, the

parameters of solution (11), and the time $t = n\,\Delta t$. The error E can be the maximum error $E_{\max}$ defined as

$$E_{\max} = \max_j |I_j^n - I(j\,\Delta s, n\,\Delta t)|$$

or the L_2 error E_{L_2} defined as

$$E_{L_2}^2 = \Delta s \sum_{j=1}^{N} |I_j^n - I(j\,\Delta s, n\,\Delta t)|^2.$$

We also compare the approximate solutions given by Eq. (28) with the exact solutions given by Eq. (11) for several different values of ν and τ. For the fourth-order method we find that $E \approx C_0\,\Delta s^4$ for both the L_2 and the maximum error, where we set $\Delta t = c\,\Delta s^2$, where $c < \frac{12}{17}$. C_0 depends on ν, τ, c, and the time $t = n\,\Delta t$.

We also compare the exact self-similar solution given by (18) with the approximate solutions obtained from Eq. (19). We find that the approximate solutions converge to the exact solution in both the maximum and L_2 norms defined above; however, the rate of convergence is lower than the second-order convergence which we obtain for smooth solutions of the self-induction equation. This is due to the fact that the self-similar solution is not smooth initially and thus the error estimates valid for smooth solutions do not apply to this case. See Figs. 1 and 2. In Fig. 3 we show the exact and calculated self-similar solutions. We observe that the tangent vectors converge strongly to the exact solution whereas the curvature and torsion of the approximate solutions converge weakly to the exact solution [12]. We have not compared the approximate self-similar solutions obtained using Eq. (28) with the exact solutions of the self-similar problem.

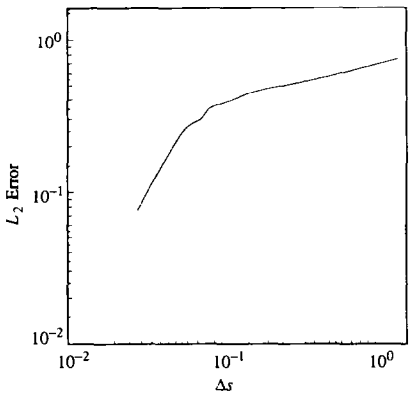

FIG. 1. The L_2 error in the self-similar solution. The L_2 error is computed in the interval $0 \leqslant s \leqslant 20.0$ at time $t = 1.0$ and plotted as a function of the mesh spacing Δs. For all points $\Delta t = \Delta s^2/2$. The approximate solutions are defined by Eq. (19) taking Eq. (12) as initial conditions.

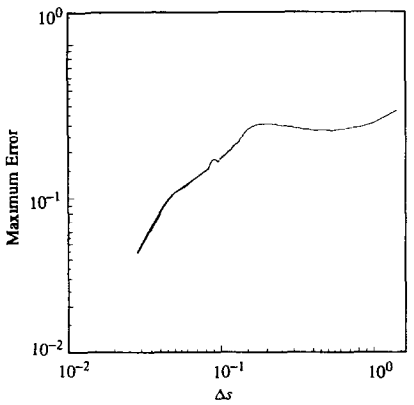

FIG. 2. The maximum error in the self-similar solution. The maximum error is computed in the interval $0 \leqslant s \leqslant 20.0$ at time $t = 1.0$ and plotted as a function of the mesh spacing Δs. For all points $\Delta t = \Delta s^2/2$ The approximate solutions are defined by Eq. (19) taking Eq (12) as initial conditions.

In concluding this section we wish to make a few comments on the numerical methods we have developed to solve the self-induction equation. The obvious features of the methods are that they are stable and satisfy several consistency properties. The methods are stable for all values of $\Delta t/(\Delta s)^2$. The unfortunate thing about Eqs. (19) and (28) is that they are implicit and must be solved iteratively. We have shown that for arbitrary initial conditions the equations can be solved provided $\Delta t < C\,\Delta s^2$. For the self-similar solution we conjecture that these conditions are also necessary for the approximate solutions to converge to the exact

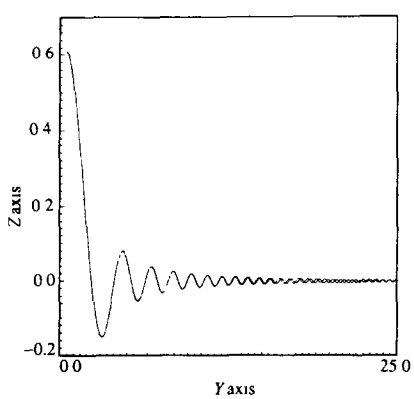

FIG 3. A comparison of the exact and calculated self-similar solution. The positive half of the self-similar vortex solution is projected onto the $y-z$ plane. Initially the vortex lies in the $x-y$ plane with I_- pointing in the negative y direction and I_+ pointing in the positive x direction. For this configuration $\kappa_0 \approx 0.4697$. The solution is shown at time $t = 1\,0$, the approximate solution is calculated with a mesh spacing $\Delta s = 0.05$ and $\Delta t = \Delta s^2/8$

solutions; the reason for this conjecture is that although Eq. (19) is an implicit scheme the numerical data propagates as if it were an explicit scheme [12]. We wish to point out, however, that these conditions can be relaxed when the initial data is smooth. For instance when calculating the solutions given by Eq. (11) we could take $\Delta t > \Delta s^2$.

VORTICES IN SUPERFLUID HELIUM

Vortices in superfluid helium are generally assumed to obey Euler's equation and thus they share some properties of vortices in an ideal fluid: the circulation of [redacted] behave completely the same as ordinary ideal vortices. In order to simplify the problem of calculating the evolution of a system of superfluid vortices Schwarz [2] introduced an approximation which depends only on the local geometry of the vortices. In Schwarz's model the superfluid vortices are assumed to obey Euler's equation with an additional force term added which models the drag that the normal component of the superfluid exerts on the superfluid component. The part of the motion determined by Euler's equation is modeled by assuming that the vortex obeys the self-induction equation (3). The drag force exerted on the vortices by the normal component is modeled by an heuristic model introduced by Hall and Vinen [13]. The result is that the motion of a superfluid vortex is assumed to obey

$$\frac{\partial \mathbf{r}}{\partial t} = \beta \mathbf{r}' \times \mathbf{r}'' + \alpha \mathbf{r}' \times (\mathbf{v}_0 - \beta \mathbf{r}' \times \mathbf{r}''). \tag{37}$$

where $'$ denotes the derivative with respect to arclength measured along the vortex, $\mathbf{r}$ is the position of the vortex, β is approximately equal to the quantum of circulation, $\alpha = \rho_n B/2\rho$ is the dimensionless friction coefficient, where B is the conventional Hall–Vinen coefficient [13], ρ_n is the normal fluid density, ρ is the total density of the fluid, and $\mathbf{v}_0$ is the local average countercurrent velocity; in Schwarz's model, which we consider here, $\mathbf{v}_0$ is assumed constant.

We can write Eq. (37) in dimensonless form by introducing dimensionless quantities by dfining $\boldsymbol{\chi} \equiv |\mathbf{v}_0|\, \mathbf{r}/\beta$ as the dimensionless position vector and in general measuring all lengths in units of $\beta/|\mathbf{v}_0|$ and by defining $\tau \equiv |\mathbf{v}_0|^2\, t/\beta$ as the dimensionless time. The resultant equation becomes

$$\frac{\partial \boldsymbol{\chi}}{\partial \tau} = \boldsymbol{\chi}' \times \boldsymbol{\chi}'' + \alpha \boldsymbol{\chi}' \times \hat{\mathbf{v}}_0 + \alpha \boldsymbol{\chi}'', \tag{38}$$

where $\hat{\mathbf{v}}_0$ is the dimensionless unit vector in the $\mathbf{v}_0$ direction and $'$ indicates differentiation with respect to dimensionless arclength. Equation (38) has also been simplified by expansion of the double cross product and the observation that $\mathbf{r}' \cdot \mathbf{r}'' = 0$.

Rather than use the natural length scale $\beta/|\mathbf{v}_0|$, Schwarz [3] introduces an arbitrary length scale which he sets equal to 1 cm.

There is no non-local interaction present in Eq. (37). Two distinct vortices governed by Eq. (37) pass through one another without experiencing any mutual influence; in order that vortices influence each other we incorporate the reconnection ansatz of Feynman [1] which states that whenever two vortices cross each other they will reconnect; see Fig. 4.

We develop a numerical method to solve Eq. (38) and incorporate the reconnection ansatz in order to determine the evolution of a system of superfluid vortices. Turbulence in superfluid helium is often characterized by determining the line length density of vortices, that is, the total length of vortices present per unit volume of fluid. We determine the line length density numerically by considering a cube of unit dimension with periodic boundary conditions and determine the total length of vortices present in the cube as a function of the countercurrent velocity $\mathbf{v}_0$. Homogeneous turbulence is characterized by the fact that the line length density is

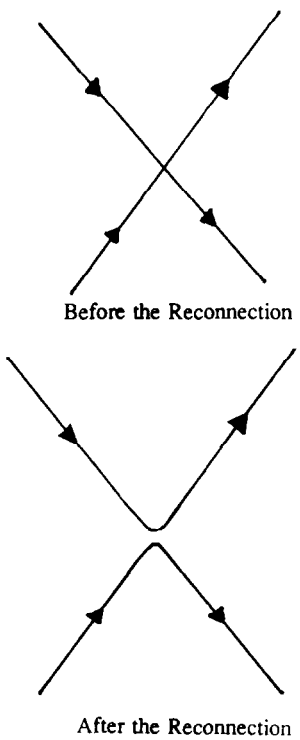

FIG. 4 The reconnection ansatz. This is a local diagram of vortices crossing immediately before and immediately after a reconnection. The algorithm does not smooth the reconnection as shown in the second diagram, but leaves a singularity there The reconnection is uniquely determined by the direction of the vorticity

proportional to $\mathbf{v}_0^2$ [3]. Our calculations show that Eq. (37) does not produce line length densities which are characteristic of homogeneous turbulence.

If we differentiate the terms of Eq. (38) with respect to ξ, the Lagrangian parametrization of the vortex, we obtain

$$\frac{\partial \mathbf{g}}{\partial \tau} = g(\boldsymbol{l} \times \boldsymbol{l}'' + \alpha \boldsymbol{l}' \times \hat{\mathbf{v}}_0 + \alpha \boldsymbol{l}''), \tag{39}$$

where $\mathbf{g} \equiv \partial \boldsymbol{\chi}/\partial \xi$, $g \equiv |\mathbf{g}| = \partial s/\partial \xi$, $\mathbf{g} = g\boldsymbol{l}$, and $'$ denotes the partial derivative with respect to the arclength s. If we assume that we have a solution $\mathbf{g}$ of Eq. (39) we can write a solution of Eq. (38) by defining $\boldsymbol{\chi}(\xi, \tau)$ as

$$\boldsymbol{\chi}(\xi, \tau) = \boldsymbol{\chi}(0, 0) + \int_0^\tau \mathbf{v}(0, \eta)\, d\eta + \int_0^s \mathbf{g}(\zeta, \tau)\, d\zeta, \tag{40}$$

where $\mathbf{v}(\xi, \tau) \equiv \boldsymbol{l} \times \boldsymbol{l}' + \alpha \boldsymbol{l} \times \hat{\mathbf{v}}_0 + \alpha \boldsymbol{l}'$. We can verify that Eq. (40) gives a solution of Eq. (38) by direct substitution.

Exact Solutions of the Model Equation

It can be shown that circular vortices are exact solutions of Eq. (38) [12]. If we specify the radius r and binormal $\mathbf{b}$ of the circular vortex as a function of time then the evolution of the circular vortex is uniquely determined. We can write the differential equations defining the evolution of the radius and binormal of the circular vortices satisfying Eq. (38) as

$$\frac{dr}{d\tau} = \cos\theta - \frac{1}{r}, \tag{41}$$

and

$$\frac{d\cos\theta}{d\tau} = \frac{1 - \cos^2\theta}{r}, \tag{42}$$

where $\cos\theta \equiv (\mathbf{b} \cdot \hat{\mathbf{v}}_0)$. For the cases $\cos\theta = \pm 1$ we solve Eq. (41) to find

$$r - r_0 + \ln\left(\frac{r-1}{r_0 - 1}\right) = \tau \qquad \text{for} \quad \cos\theta = 1, \tag{43}$$

and

$$-(r - r_0) + \ln\left(\frac{r+1}{r_0 + 1}\right) = \tau \qquad \text{for} \quad \cos\theta = -1, \tag{44}$$

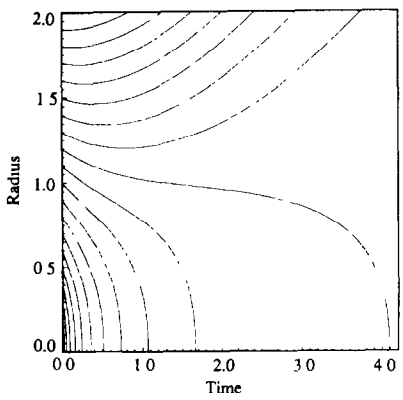

FIG. 5. Radius as a function of time for a circular vortex. The radius of a circular vortex evolving according to Eq. (37) is plotted as a function of time for various initial radii with $\cos\theta = 0.5$ initially.

where r_0 is the initial radius of the vortex. From (43) we see that if $\cos\theta = 1$ the radius decreases to zero in finite time provided $r_0 < 1$; for $\cos\theta = -1$ from (44) we see that the radius decreases to zero in finite time for all r_0. The solutions of Eqs. (41) and (42) for arbitrary initial conditions are similar to the solution given by Eq. (43) except for the fact that $\cos\theta$ is an increasing function of time provided $|\cos\theta| \neq 1$ initially. For small r_0 the radius decreases to zero in finite time and for large r_0 the radius increases asymptotically linearly in time. See Fig. 5. The important fact about circular solutions is that all circular solutions decrease to zero in finite time provided that $r_0 < 1$.

For a general solution of Eq. (38) the length of the vortex decreases in regions where the curvature $\kappa > 1$; we can see this by multiplying both sides of Eq. (39) by $\mathbf{g}$ to obtain

$$\frac{\partial g}{\partial \tau} = \alpha g \kappa (\mathbf{b} \cdot \hat{\mathbf{v}}_0 - \kappa), \tag{45}$$

where we use the Frenet–Serret formula to simplify the right side of Eq. (39).

THE FINITE DIFFERENCE EQUATIONS

We now introduce a set of finite difference equations to approximate Eq. (39). We view Eq. (39) as a perturbation of Eq. (6); however, it is no longer possible to take the arclength as the Lagrangian parametrization of the vortex since the

arclength of a vortex evolving according to Eq. (39) is a function of time. Our finite difference equation approximating Eq. (39) is

$$\mathbf{g}_j^{n+1} - \mathbf{g}_j^n = \frac{\Delta\tau}{4\Delta\xi^2}\mathbf{l}_j \times (h_{j+1}\mathbf{l}_{j+2} + h_{j-1}\mathbf{l}_{j-2}) + \alpha\frac{\Delta\tau}{2\Delta\xi}(\mathbf{l}_{j+1} - \mathbf{l}_{j-1}) \times \hat{\mathbf{v}}_0$$

$$+ \alpha\frac{\Delta\tau}{4\Delta\xi^2}(h_{j+1}\mathbf{l}_{j+2} - (h_{j+1} + h_{j-1})\mathbf{l}_j + h_{j-1}\mathbf{l}_{j-2}), \tag{46}$$

where $\Delta\tau$ is the time step, $\Delta\xi$ is the distance between mesh points, $\mathbf{g}_j^n$ is an approximation to $\mathbf{g}(j\Delta\xi, n\Delta\tau)$, $\mathbf{g}_j \equiv (\mathbf{g}_j^n + \mathbf{g}_j^{n+1})/2$, $h_j \equiv 1/|\mathbf{g}_j|$, and $\mathbf{l}_j \equiv h_j\mathbf{g}_j$. Note that $|\mathbf{l}_j| = 1$. Equation (46) follows from Eq. (38), the fact that $\partial/\partial s = (1/g)(\partial/\partial\xi)$, and the second-order difference operator

$$\frac{\partial}{\partial\xi}\left(u\frac{\partial w}{\partial\xi}\right) \approx \Delta_0(u\,\Delta_0 w)$$

$$= \frac{1}{4\Delta\xi^2}(u_{j+1}w_{j+2} - w_j(u_{j+1} + u_{j-1}) + u_{j-1}w_{j-2}),$$

where Δ_0 is the central divided difference operator. Equation (46) is designed so that the first two invariants (20) and (21) of the self-induction scheme (19) are preserved by Eq. (46) when $\alpha = 0$. Consider Eq. (46) for the case $\alpha = 0$, then when we multiply the terms of Eq. (46) by $(\mathbf{g}_j^{n+1} + \mathbf{g}_j^n)$ we obtain that

$$|\mathbf{g}_j^{n+1}|^2 - |\mathbf{g}_j^n|^2 = 0.$$

Thus the self-induction part of the numerical scheme introduces no stretching or contraction of the vortex. The second invariant is preserved even for the case when $\alpha \neq 0$. The invariant is

$$\sum_{j=1}^{N} \mathbf{g}_j^{n+1} = \sum_{j=1}^{N} \mathbf{g}_j^n, \tag{47}$$

where we have assumed periodic boundary conditions. Equation (47) can be verified by summing the terms of Eq. (46) and noting that the terms appearing on the right side of the equation form a telescoping series. Equation (47) guarantees that vortices which are closed initially remain closed for all times when we define the approximation to $\mathbf{r}(j\Delta\xi, (n+1)\Delta t)$, which we denote as $\mathbf{r}_j^{n+1}$, as

$$\mathbf{r}_j^{n+1} = \mathbf{r}_0^0 + \Delta t \sum_{m=1}^{n} \mathbf{v}_0^{m+1/2} + \frac{\Delta\xi}{2}\sum_{i=1}^{j}(\mathbf{g}_{i-1}^{n+1} + \mathbf{g}_i^{n+1}), \tag{48}$$

where

$$\mathbf{v}_j^{n+1/2} = \frac{1}{2\Delta\xi}h_j\mathbf{l}_j \times (\mathbf{l}_{j+1} - \mathbf{l}_{j-1}) + \alpha\mathbf{l}_j \times \mathbf{v}_0 + \frac{\alpha}{2\Delta\xi}h_j(\mathbf{l}_{j+1} - \mathbf{l}_{j-1}),$$

with the quantities defined as in Eq. (46). With these definitions method (48) for approximating Eq. (37) is formally second-order accurate in space and time.

The third invariant is not preserved exactly, but an expression analogous to Eq. (22) can be written down for solutions of Eq. (46). For the case $\alpha = 0$ it can be shown that

$$\sum_{j=1}^{j=N} (h_{j-1}(\mathbf{l}_j - \mathbf{l}_{j-2}) \cdot ((\mathbf{g}_j^{n+1} - \mathbf{g}_{j-2}^{n+1}) - (\mathbf{g}_j^n - \mathbf{g}_{j-2}^n))) = 0$$

for periodic boundary conditions, where the quantities appearing are defined in Eq. (46).

We solve Eq. (46) by means of an iterative method analogous to the one given in Eq. (23). We do not use the normalization step as given in (24) since the $\mathbf{g}_j^n$ for which we are solving in Eq. (46) change their magnitude. We formally write the method for solving Eq. (46). Let $\mathbf{F}_j(\cdot, \cdot)$ be defined so that Eq. (46) can be rewritten as

$$\mathbf{g}_j^{n+1} - \mathbf{g}_j^n = \mathbf{F}_j(\mathbf{g}^n, \mathbf{g}^{n+1}),$$

where $\mathbf{g}^n$ and $\mathbf{g}^{n+1}$ denote the dependence of $\mathbf{F}_j$ on the $\mathbf{g}_i^n$ and $\mathbf{g}_i^{n+1}$ for $1 \leqslant i \leqslant N$. We define a sequence $\tilde{\mathbf{g}}^k$ given $\mathbf{g}_j^n$ by means of the equation

$$\tilde{\mathbf{g}}_j^{k+1} - \mathbf{g}_j^n = \mathbf{F}_j(\mathbf{g}^n, \tilde{\mathbf{g}}^k), \tag{49}$$

where we chose $\tilde{\mathbf{g}}_j^0 = \mathbf{g}_j^n$. Numerically we find that $\tilde{\mathbf{g}}_j^k$ converges to a vector which satisfies Eq. (46) for all $\mathbf{g}_j^n$ provided

$$\frac{\Delta\tau}{\Delta\xi^2} < \frac{1}{4}, \tag{50}$$

and

$$\min_j |\mathbf{g}_j^n| > \tfrac{1}{2}.$$

Thus we define $\mathbf{g}_j^{n+1} \equiv \lim_{k \to \infty} \tilde{\mathbf{g}}_j^k$.

Equation (46) is valid for any Lagrangian parametrization of the vortex; however, if we choose as our parametrization the initial arclength of the vortex then, at least initially, the approximation points are uniformly spaced along the vortex. As the vortex evolves the approximation points will not remain uniformly spaced, but will become bunched together in regions where the vortex contracts and they will become spread apart in regions where the vortex stretches. We can monitor the distance between approximation points by monitoring $|\mathbf{g}_j^n|$ at each time step. If we take initial arclength as our parametrization then $|\mathbf{g}_j^0| = 1$. If $|\mathbf{g}_j^n|$ becomes too large we introduce additional approximation points so that the distance between approximation points remains close to the initial value $\Delta\xi$. If $|\mathbf{g}_j^n|$ becomes too small we have approximation points which are too closely spaced and even-

tually condition (50) will not be satisfied and we will not be able to find a solution to Eq. (46).

There are a number of ways of introducing more approximation points, for instance, see Anderson and Greengard [14]; we choose a method due to Chorin [8] for spacing the points. If the magnitude of a vector $\mathbf{g}_j^n$ is greater than a certain length $l_{\max}$, we divide the vector in half and track the two vectors individually. The vector $\mathbf{g}_j^n$ is replaced by two vectors $\mathbf{g}_{j-1/2}^n$ and $\mathbf{g}_{j+1/2}^n$, where $\mathbf{g}_{j-1/2}^n = \mathbf{g}_{j+1/2}^n = \mathbf{g}_j^n/2$. It may also happen that $|\mathbf{g}_j^n|$ becomes smaller than some constant $l_{\min}$, if this happens we replace the vectors $\mathbf{g}_j^n$ and $\mathbf{g}_{j+1}^n$ by the vector $\mathbf{g}_j^n + \mathbf{g}_{j+1}^n$. After each time step we check the lengths of the $\mathbf{g}_j^{n+1}$ and add and delete points according to the description given above so that at the beginning of each time step we have

$$l_{\min} \leqslant |\mathbf{g}_j^n| \leqslant l_{\max} \qquad \text{for all } j.$$

In our algorithm we choose $l_{\min} = \frac{1}{2}$ and $l_{\max} = \sqrt{2}$.

We determine if it is necessary to reconnect vortices by monitoring the distance between any two mesh points. If the distance between any two points is less than $\Delta\xi$, we save these points as a possible candidate for a reconnection. We then check all of the points in the neighborhood of the possible candidate and choose the pair of points which is the minimum distance apart and reconnect only the pair which is the minimum distance apart in a given neighborhood. Once we have chosen a pair of points for a reconnection we do not allow another reconnection within a distance of $6\Delta\xi$. We reconnect two points by redefining the two designated tangent vectors so that their nearest neighbors' positions are unchanged. As we shall see in the following section, the details of the reconnection are unimportant as long as the spacing of the mesh is small enough. On the other hand if the spacing is too large, there is no way to reconnect the vortices correctly since small perturbations in the way in which one reconnects the vortices will make large changes in the resultant vortex configuration; i.e., the resultant initial value problem is ill-posed.

Numerical Results

The truncation error in the numerical method and the resolution needed near the kinks in the vortices when they reconnect are carefully analyzed. Empirically, it is found that the mesh point spacing along the vortex $\Delta\xi$, must satisfy

$$\Delta\xi \leqslant 0.5,$$

where $\Delta\xi$ is measured in the appropriate dimensionless units, in order that the numerical solutions accurately represent the exact solutions. The calculations of Schwarz violate this criterion at high velocities and by repeating his calculations with a finer grid it is found that the results disagree with his work; it is found that the line length density of the vortex tangle is not proportional to the velocity

squared. It is concluded that the model used is inadequate to describe turbulence in superfluid helium.

The only exact solutions of the complete equation (38) which are known are the solutions given by Eqs. (41) and (42). We have compared our approximate solutions obtained with Eq. (46) with the exact solutions and find that the approximate solutions converge to the exact solutions. These trivial solutions evolve in time only by changing their radius and orientation relative to $\mathbf{v}_0$ and are only of limited value in verifying a numerical scheme; the solutions have a curvature which is constant in space and a torsion which is identically zero. Thus these solutions cannot be expected to give a good indication of how the numerical method will work in general. The best test which can be performed on the full equation is to investigate the numerical solutions as the mesh spacing is decreased for initial conditions, in which the vortex contains a kink and is not planar. It is found that as the spacing between mesh points is sufficiently reduced the numerical solutions remain invariant. What is of crucial significance in the present context, however, is that the character of the numerical solutions changes drastically as the mesh changes from a coarse one to a finer one. If the mesh is too coarse it is observed that there is a spurious creation of vortex loops emanating from the point of reconnection. Once the mesh is refined below a certain threshold the spurious generation ceases and the solution converges rapidly [12]. In Fig. 6a we show the vortex which results from the reconnection of two vortices in which the mesh spacing $\Delta\xi = 4.0$; in Fig. 6b we show the result of the reconnection from the same initial conditions as in Fig. 6a except that $\Delta\xi = 0.5$. The converged result is the same as that shown in Fig. 6b.

We emphasize that this spurious generation of vortex loops is not peculiar to our algorithm. We have implemented Schwarz's algorithm as given in [15] and find the

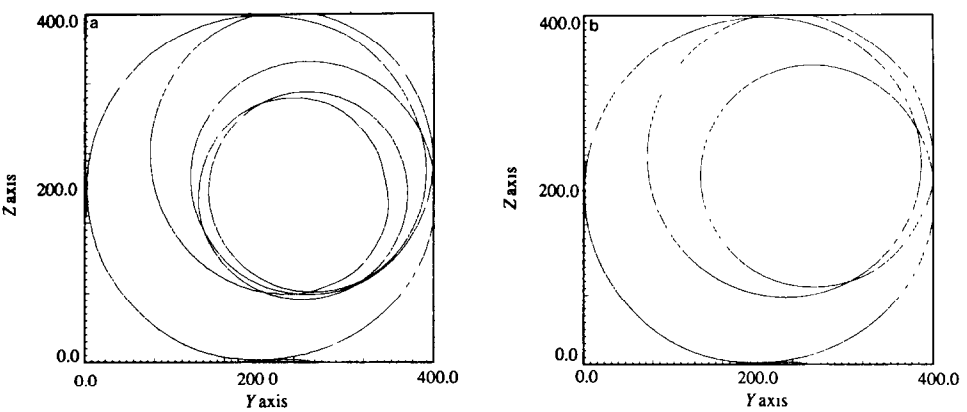

FIG 6. (a) Projection of a vortex after it has undergone a reconnection Two perpendicular circular vortices are allowed to reconnect at time $\tau = 0$ and the resultant vortex is shown at time $\tau = 1600.0$. The mesh spacing is $\Delta\xi = 4.0$ and $\Delta\tau = 1.6$. The vortex is projected onto the $y-z$ plane (b) The same conditions as in (a) except that the mesh spacing is $\Delta\xi = 0.5$ and $\Delta\tau = 0.01625$

same behaviour. In Fig. 7 we show the results of a reconnection obtained with Schwarz's algorithm. Fig. 7a shows the initial conditions. Figures 7b and 7c show the resultant vortex at times $t=0.1$, 0.2, respectively, calculated with a mesh spacing corresponding to $\Delta\xi=4.0$. In Figs. 7c–f we show the resultant vortex at time $t=0.2$ with different mesh spacings and time increments. We see that if reconnections were allowed to continue one would obtain five vortices for large mesh spacings, whereas the correct result would show only one large vortex.

Almost without fail when the mesh is too coarse, spurious vortex loops will be created at the point of reconnection, whereas if the vortex is properly resolved a vortex loop will be formed at the point of reconnection only rarely. From Eq. (45) we see that at the reconnection point (a region of arbitrarily large curvature) the vortex should contract and vortex loops should not be formed.

We analyze the origin of this threshold mesh size. The spurious vortex growth occurs when the numerical algorithm cannot accurately approximate a curvature, in reduced units, larger than one, causing the vortex to stretch numerically rather than contract as required by the exact solution. The condition which guarantees that the numerics accurately approximates the exact solution is that the mesh size be chosen so that curvatures much larger than one can be accurately evaluated. The curvature is given by

$$|\kappa| \approx \left| \frac{1}{g_j} \frac{\boldsymbol{l}_{j+1} - \boldsymbol{l}_{j-1}}{2\Delta\xi} \right|.$$

A reasonable uniform mesh spacing along the vortex such that g_j is of order unity requires as the condition for accurate solutions of high curvature that

$$\Delta\xi \ll 1.$$

Empirically, after careful convergence studies, we find the actual numerical condition to be

$$\Delta\xi \leqslant 0.5 \tag{51}$$

for the vortex tangle calculations. We emphasize that the value 0.5 is only valid for the specific numerical algorithm considered here. Less robust and less accurate algorithms may require a more severe restriction on the spatial mesh as well as an auxilary restriction on the time step. Note the dependence on Δt in Figs. 7d–f.

We calculated the line length in a cube with sides of length L with periodic boundary conditions as a function of $\gamma \equiv L|\mathbf{v}_0|/\beta$. We start the calculation with simple initial conditions generally consisting of four circular vortices. The length of the vortices is calculated at each time step as they evolve. It is found that eventually the length reaches an equilibrium value and simply fluctuates about an average value.

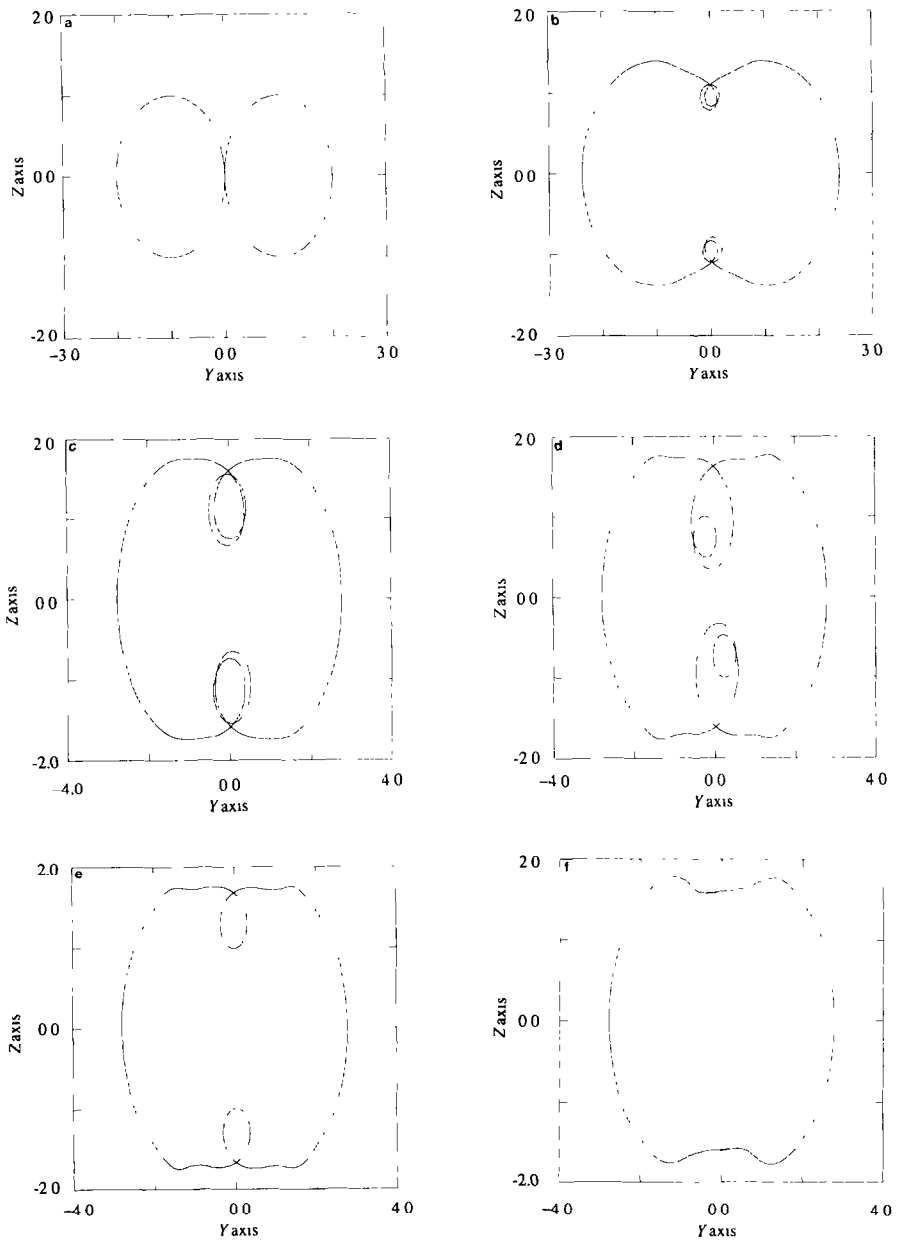

FIG. 7. (a) The vortex initially. The evolution of a vortex after a reconnection is calculated according to the algorithm given in [15]. $\mathbf{v}_0$ is parallel to the x-axis. The units Δt and Δr used in Fig. 7 are the same as those given in [3]. They are related to the units defined in Eq. (46) by $\Delta\tau = |\mathbf{v}_0|^2\,\Delta t$ and $\Delta\xi = \Delta r\,|\mathbf{v}_0|$. (b) The vortex at time $t = 0.1$, $\Delta r = 0.1$, $\Delta t = 0.0002$, $\alpha = 0.1$, $|\mathbf{v}_0| = 40.0$. (c) The vortex at time $t = 0.2$, $\Delta r = 0.1$, $\Delta t = 0.0002$, $\alpha = 0.1$, $|\mathbf{v}_0| = 40.0$. (d) The vortex at time $t = 0.2$, $\Delta r = 0.05$, $\Delta t = 0.0002$, $\alpha = 0.1$, $|\mathbf{v}_0| = 40.0$. (e) The vortex at time $t = 0.2$, $\Delta r = 0.05$, $\Delta t = 0.0001$, $\alpha = 0.1$, $|\mathbf{v}_0| = 40.0$. (f) The vortex at time $t = 0.2$, $\Delta r = 0.05$, $\Delta t = 0.00005$, $\alpha = 0.1$, $|\mathbf{v}_0| = 40.0$

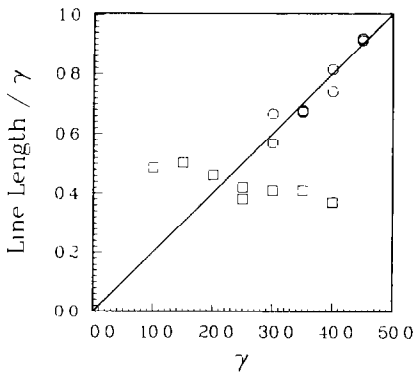

FIG. 8. Average line length in a cube of side L as a function of the countercurrent velocity, $\gamma = L|\mathbf{v}_0|/\beta$. The line lengths represented by the squares were calculated with $\Delta\xi \leqslant 0.5$; the line lengths represented by the octagons were calculated with $\Delta\xi = \Delta r\,|\mathbf{v}_0|/\beta \geqslant 0.6$ for two different conditions, with Δr fixed and $\alpha = 0.10$. The straight line corresponds to the results given in Ref. [3]. The average line length is given in units of L.

The time average of the lengths are shown in Fig. 8 by the squares, indicating line lengths which are nearly linearly dependent on the velocity. The line length density, on the other hand, scales as the velocity squared indicating homogeneous turbulence in the earlier numerical work [3] and this result is indicated by the straight line passing through the origin. We note that although the line length densities for the finer mesh are not characteristic of homogeneous turbulence, the vortex tangles are spatially uniform as shown in Fig. 9. We have calculated the line length densities for several different values of α and we find that the previous calculations [3] of line length density are incorrect [12].

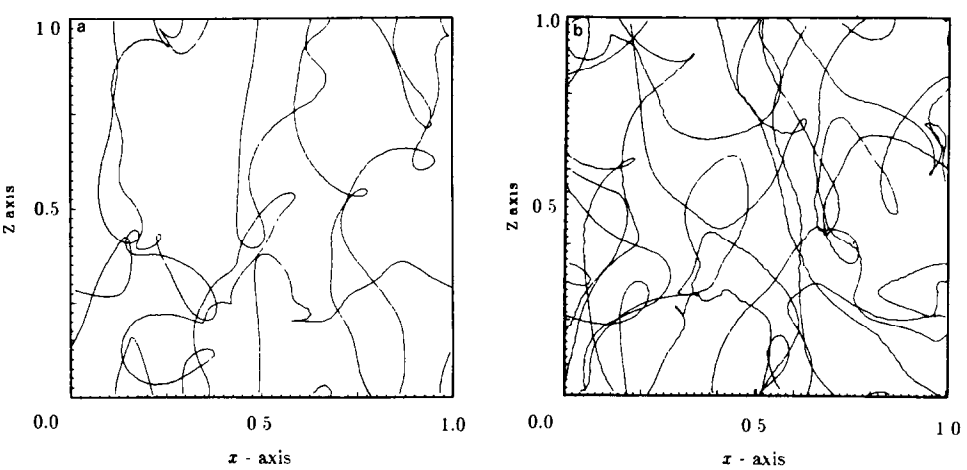

FIG. 9. (a) A typical vortex tangle projected onto the $x-z$ plane. $\mathbf{v}_0$ points in the positive x direction, $\alpha = 0.10$, $\Delta\xi = 0.5$, $\gamma = 40.0$. (b) The same initial conditions except that $\Delta\xi = 0.8$. The increase in line density over that present in Fig. 9a is readily apparent.

We now see why the correct length scaling is so important in this problem. Physically one thinks of increasing $\mathbf{v}_0$, the countercurrent velocity, for given initial conditions. In this process the requirement that $\Delta\xi \leqslant 0.5$ will be violated unless the mesh size is refined as the velocity increases. We have reproduced the earlier results of Schwarz for a fixed mesh independent of velocity, which leads to a violation of the requirement that $\Delta\xi \leqslant 0.5$. These are the results one obtains if one does not make Eq. (37) dimensionless or if one does it incorrectly. We pick $\Delta\xi \equiv \Delta r\, |\mathbf{v}_0|/\beta$ and keep Δr fixed rather than $\Delta\xi$. Thus we are effectively calculating with a coarser mesh as $|\mathbf{v}_0|$ is increased. This is the calculation Schwarz has done in [3] by scaling Eq. (37) incorrectly. These results are shown in Fig. 8 by the octagons for two different initial conditions. The line in Fig. 8 is the one given in [3].

Conclusion

We have shown that the line lengths previously reported in [3] were a result of the incorrect scaling of the model equation (37) and as a result, an underresolved computational mesh. The fact that we were able to reproduce the erroneous results of [3] indicates that the erroneous results are insensitive to the exact number of loops that are produced at a reconnection and that the ultimate line length density present is determined by the geometry of the tangle in the regions of small curvature, i.e., away from the reconnection points. This seems to indicate that the term which models the drag on the superfluid vortices is correct, but that the term which models the self-induced motion of the vortices is incorrect. The fact that more vortices (at a small scale) have to be introduced in order to produce a scaling which is characteristic of homogeneous turbulence suggests that a successful model must include some stretching terms which are present in the evolution of a vortex in an ordinary fluid as given by Eq. (1). These observations are consistent with what is known in the theory of vortex motion in classical fluids [8, 9].

Equation (37) is inadequate for a description of turbulence in superfluid helium. It is clear that self-induction is inadequate to describe the classical motion of the vortex even in the superfluid case. Models to describe superfluid helium turbulence will have to maintain more of the non-local character of Euler's equation than self-induction does. The self-induction term even with the reconnection ansatz included is inadequate to model the evolution of a turbulent vortex.

Acknowledgments

The author acknowledges numerous helpful discussions with Alexandre Chorin. The author also acknowledges the Computer Facilities and Communications department at Berkeley for the use of the IBM 3081 computer. This work was suported in part by the Applied Mathematics Subprogram of the Office of Energy Research, U S. Department of Energy under Contract DE-AC03-76SF00098 at the Lawrence Berkeley Laboratory.

REFERENCES

1. R. P. FEYNMAN, "Application of Quantum Mechanics to Liquid Helium," in *Progress in Low Temperature Physics*, (North-Holland, Amsterdam, 1955), Vol. 1.
2. K. W SCHWARZ, *Phys Rev. B* **18**, 245 (1978).
3. K W SCHWARZ, *Phys Rev. Lett* **49**, 283 (1982)
4. A J. CHORIN AND J MARSDEN, *A Mathematical Introduction to Fluid Mechanics*, (Springer-Verlag, New York, 1979).
5. F. R. HAMA, *Phys. Fluids* **5**, 1156 (1962).
6. F R. HAMA, *Phys. Fluids* **6**, 526 (1963).
7. G. K BATCHELOR, *An Introduction to Fluid Dynamics* (Cambridge Univ. Press, London, 1967).
8. A. J. CHORIN, *Commun Math. Phys.* **83**, 517 (1982).
9. E. SIGGIA, *Phys. Fluids* **28**, 794 (1985).
10. H. HASIMOTO, *J. Fluid Mech.* **51**, 477 (1972).
11. A. C NEWELL, *Solitons in Mathematics and Physics* (SIAM, Philadelphia, 1985).
12. T F. BUTTKE, Thesis, University of California, Berkeley, LBL Report LBL-22086, 1986 (unpublished)
13. H. E HALL AND W. F. VINEN, *Proc. R Soc. A* **238**, 204 (1956).
14. C ANDERSON AND C. GREENGARD, *SIAM J. Numer. Anal.* **22**, 413 (1985).
15. K. W SCHWARZ, *Phys. Rev B* **31**, 5782 (1985).